Inorganic Chemistry

pubs.acs.org/IC

Article

Tuning Cu Overvoltage for a Copper−Telluride System in Electrocatalytic Water Reduction and Feasible Feedstock Conversion: A New Approach

Sangeetha Kumaravel, Kannimuthu Karthick, Prabaharan Thiruvengetam, Jinta Merlin Johny, Selvasundarasekar Sam Sankar, and Subrata Kundu*

Cite This: https://dx.doi.org/10.1021/acs.inorgchem.0c01648

Read Online

ABSTRACT: Highly efficient and earth-abundant elements capable of water reduction by electrocatalysis and are attractive for the sustainable generation of fuels. Among the earth-abundant metals, copper is one of the cheapest but often the most neglected choice for the hydrogen evolution reaction (HER) due to its high overvoltage. Herein, for the first time we have tuned the overpotential of copper by tellurizing it by two different methodologies, viz. hydrothermal and wet chemical methods, which form copper telluride nanochains and aggregates. The application of copper telluride as an electrocatalyst for the HER gave fruitful results in terms of both activity and stability. The hydrothermally synthesized catalyst $Cu_{2-x}Te$/hyd shows a low overpotential (347 mV) at 10 mA cm^{-2} toward the HER. In addition, the catalyst showed a very low charge transfer resistance (R_{ct}) of 24.4 Ω and, as expected, $Cu_{2-x}Te$/hyd exhibited a lower Tafel slope value of 188 mV/dec in comparison to $Cu_{2-x}Te$/wet (280 mV/dec). A chronoamperometry study reveals the long-term stability of both catalysts even up to 12 h. The Faradaic efficiency of $Cu_{2-x}Te$/hyd was calculated and found to be 95.06% by using gas chromatographic (GC) studies. Moreover, with the idea of utilizing produced hydrogen (H_2) from electrocatalysis, for the first time we have carried out feedstock conversion to platform chemicals in water under eco-friendly green conditions. We have chosen cinnamaldehyde, 2-hydroxy-1-phenylethanone, 4-(benzyloxy)benzaldehyde, and 2-(3-methoxyphenoxy)-1-phenylethanone (β-O-4) as model compounds for feedstock conversion by hydrogenation and/or hydrogenolysis reactions in aqueous medium using external hydrogen pressure. This protocol could also be scaled up for large-scale conversion and the catalyst is likely to find industrial application since it requires an inexpensive catalyst and an easily available, mild reducing agent. The robustness of the developed catalyst is proven by recyclability experiments and its possibility of use in real-life applications.

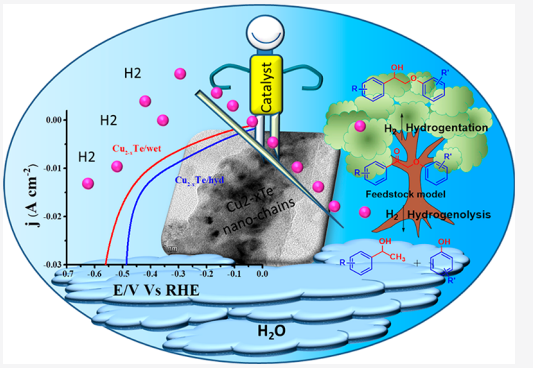

INTRODUCTION

Globalization and increasing demands in all most every sector have strongly driven the scientific community to find alternative technologies.[1,2] Particularly, energy scarcity creates a significant transition toward clean and effective energy resources.[2−6] Hydrogen (H_2) production from water electrolysis is the ultimate green and clean renewable energy resource for the future and is a better alternative to fossil fuels, which produce more CO_2 in the atmosphere.[1,4,7−10] In addition, energy production from finite, nonrenewable fossil fuels reserves is perceived to be unsustainable in the long run. Therefore, hydrogen production from water electrolysis is considered as one of the optimum ways among the other available methods and produces water as the sole byproduct.[7] However, efficient water electrolysis is possible only when the catalyst for the hydrogen evolution reaction is affordable, environmentally benign, and earth abundant. Therefore, the judicious choice of a cheaper element with low overvoltage that is capable of large-scale H_2 production would constitute the foremost criterion in developing efficient water reduction.[11,12]

In general, the half-cell reaction of water electrolysis involves the hydrogen evolution reaction (HER) at the cathode and the oxygen evolution reaction (OER) at the anode which are catalyzed by Pt,[13] IrO_2/RuO_2,[14−16] and their alloys. The aforementioned expensive standard electrocatalysts are a barrier to the large-scale production of H_2. To replace this state of the art catalyst by atom economy with high efficiency is considered to be the next stage in energy production.[17−21] With a focus on cost-effective catalysts, several studies have

Received: June 4, 2020

utilized the 3d transition metals, in particular Fe,[22−28] Co,[18,29−32] and Ni,[17,20,21,26,33] for the hydrogen evolution reaction in both acidic and alkaline medium. In addition in the 3d transition-metal series, oxides,[18,20,23,29] mixed metal oxides,[23,34,35] hydroxides,[29,36,37] nitride,[38,39] carbide,[33,40] phosphide[12,41−43] and layered double hydroxide[27,44] (LDH) materials have been well studied. Even though the efficiency of this 3d transition-metal series in the HER is satisfactory, further advances are needed. Therefore, to increase the electrocatalyst performance for the HER, non-noble-metal chalcogenide materials such as sulfides,[11,30,45,46] selenides,[8,11,26,32,47,48] and tellurides[17,48] have been incorporated with these transition metals and show superior electrochemical activities in the HER. In recent literature, research has been focused on selenization and sulfurization with transition metals to improve the HER rate.[11] Alshareef *et al.* carried out selenization of phase-, surface-, and morphology-engineered NiCo nanomaterials which results in tremendous activity in the HER with high stability.[32] The tellurides of transition-metal-based catalysts showed good HER activities. For an examples, nickel tellurides prepared by Bhat *et al.* showed an overpotential of 679 mV and a Tafel slope of 151 mV/dec.[49] In another interesting work by Wang *et al.*, $CoTe_2$ nanostructures on carbon fiber paper were prepared and required a much lower overpotential of 230 mV at 100 mA cm^{-2}. Further, it also delivered high stability even after 5000 cycles and 20 h of prolonged exposure.[50] In an another work by Lu *et al.*, $CoTe_2$ nanostructures with a diameter range of 20−50 nm were prepared and showed an overpotential of 246 mV at a current density of 10 mA cm^{-2}.[51]

In this regard, copper (Cu) is the most abundant and cheapest element in earth for development of an electrocatalyst.[22−25] Even though Cu is more earth abundant, its higher overvoltage makes it an unsuitable element for the HER process. In the literature, copper has been utilized with equimolar amounts of other noble metals such as Pt, Ag, and Au to enhance the HER activity.[18,23] Also, to reduce the HER overpotential of Cu, selenization, phosphorization, and sulfurization were carried out by using several protocols; however, the preparation procedure is difficult and/or environmentally unfriendly.[18,22,24,29] To overcome this issue, a suitable metal partner with Cu is essential to increase the HER activity of Cu. Along this line, our group proved that selenization of Cu foam shows higher HER activity than pristine copper foam.[24] Lu *et al.* have developed Cu_3P nanowires by a simple one-step phosphorization, resulting in a huge increase in the HER performance.[52] Therefore, considering the above discussion, we made an attempt to tellurize copper using hydrothermal and wet chemical methods to study the HER activity.

In addition, the dual advantage of the developed catalyst was planned to utilize for fine chemical synthesis the conversion of feedstock materials derived from agricultural waste products using hydrogen produced via water electrolysis. The use of both hydrogenation and hydrogenolysis reactions of feedstock conversion using hydrogen gas is tuned by an identical catalyst has been limited in reports.[25,53,54] Recent reports highlighted the utilization of oxygen produced from electrocatalytic water splitting for the oxidation of alcohol.[55] Jiang *et al.* developed a $CeO_2/ZnIn_2S_4$ hybrid for the selective oxidation of aromatic alcohols coupled with hydrogen evolution, which highlighted the dual approach in the production of fine chemicals and H_2 evolution.[56,57] Ko *et al.* recently reported photoelectrobiochemical feedstock conversion. In this study, the in situ generated H_2O_2 from a three-compartment photoelectrobiochemical reactor has been utilized for stable and selective lignin valorization.[58] To the best of our knowledge, there has been no report on feedstock conversion by using in situ generated H_2. We are proposing the idea of utilizing the electrochemically generated H_2 in feedstock conversion. A detailed comparison of our protocol with available literature methods is provided under the section 'Catalytic Hydrogenation/Hydrogenolysis of Feedstock Model Compound' below.

In this work, for the first time we have successfully developed copper telluride nanochains and aggregates for HER under aqueous acidic conditions. Also, the performance of these $Cu_{2-x}Te$ nanochains and aggregates in the HER was comparatively investigated by varying the synthetic methodology by hydrothermal and wet-chemical methods. These comparative results strongly imply that the catalyst prepared by the hydrothermal method ($Cu_{2-x}Te$/hyd) exhibits activity superior to that of the wet chemical method ($Cu_{2-x}Te$/wet) toward the HER. The HER overpotential of $Cu_{2-x}Te$/hyd nanochains is 347 mV to attain 10 mA cm^{-2} with a low Tafel slope value of 188 mV/dec. $Cu_{2-x}Te$/hyd exhibits low charge transfer resistance and long-term stability in comparison to $Cu_{2-x}Te$/wet. Here for the first time, an earth-abundant and cost-effective metal catalyst for hydrogen production and the idea of its utilization in environmentally friendly feedstock conversion by hydrogenation and/or hydrogenolysis reactions toward various useful chemicals on a large scale by simply changing reaction conditions in aqueous medium under external hydrogen pressure is demonstrated. We have chosen cinnamaldehyde, 2-hydroxy-1-phenylethanone, 4-(benzyloxy)-benzaldehyde, and 2-(3-methoxyphenoxy)-1-phenylethanone (β-O-4 linkage) as model compounds for the selective and large-scale conversion of feedstock components by hydrogenation and/or hydrogenolysis reactions in water under external hydrogen pressure.

EXPERIMENTAL METHODS

Synthesis of $Cu_{2-x}Te$ Nanochains and Aggregates. *Hydrothermal and Wet Chemical Methods of Synthesis.* The efficient synthetic methodology to designing a unique and cost-effective catalyst for the HER is as follows. In order to synthesize the $Cu_{2-x}Te$ nanochains and aggregates, hydrothermal and wet chemical methodologies were carried out (Scheme S1). Here, in the hydrothermal method of tellurizing copper, the reaction of $NaBH_4$ with Te powder was carried initially. In detail, freshly prepared 0.1 M ice-cold $NaBH_4$ was added along with 0.01 M tellurium powder, and the reaction mixture was heated at 80 °C with gentle stirring for about 15 min; this resulted in the nucleation of NaHTe. After the immediate formation of NaHTe, it was further reacted with 0.02 M copper metal ions from $CuCl_2{\cdot}2H_2O$. The probable mechanism in the $Cu_{2-x}Te$ formation is discussed in detail as

$$2Te + 2NaBH_4(aq) + 2H_2O \rightarrow 2NaHTe(aq) + 2B(OH)_4^-(aq) + H_2(g)$$

$$2NaHTe(aq) + Cu^{2+}(s) \rightarrow Cu_{2-x}Te + 2H^+(aq) + 2Na^+(aq)$$

After that, the whole solution mixture was transferred into a 50 mL Teflon-lined autoclave vessel and kept in a furnace at 180 °C for a quick time of 3 h. This treatment resulted in a black precipitate that was washed thoroughly with water and dried at 80 °C for 5 h. The obtained black powder shows the successful tellurization of copper to form $Cu_{2-x}Te$ nanochains and is named $Cu_{2-x}Te$/hyd. Following the same procedure, the wet chemical method of synthesizing $Cu_{2-x}Te$

https://dx.doi.org/10.1021/acs.inorgchem.0c01648
Inorg. Chem. XXXX, XXX, XXX−XXX

nanoaggregates was performed. Here the reaction mixture of 0.1 M freshly prepared ice-cold $NaBH_4$ with Te powder was stirred for 30 min under mild heating conditions and at a certain time a change in the intense black of tellurium to light black showed the nucleation of NaHTe. To this was added 0.02 M $CuCl_2 \cdot 2H_2O$, and this mixture was continuously stirred for 10 min to give a black precipitate. The resulting black precipitate was washed thoroughly with water and dried in an oven for 8 h at 80 °C. The $Cu_{2-x}Te$ nanoaggregates prepared by this wet chemical method were named $Cu_{2-x}Te$/wet. The prepared materials were confirmed by various characterization techniques and used for electrochemical HER studies in acidic medium. Details of the materials used and sample preparation techniques for characterization are given in the Supporting Information.

General Procedure in Electrode Fabrication for HER Studies. The performance of $Cu_{2-x}Te$ nanochains and aggregates prepared by hydrothermal and wet chemical synthesis, respectively, has been studied for the HER in 0.5 M H_2SO_4. A typical three-electrode system was adapted to study the HER with carbon cloth as the counter electrode, Hg/Hg_2SO_4 as the reference electrode, and $Cu_{2-x}Te$-coated carbon cloth as the working electrode. Linear sweep voltammetric (LSV) curves were obtained at a scan rate of 5 mV s^{-1} after activation. A long-term chronoamperometry study was done at a current density of 10 mA cm^{-2} for 12 h. All of the LSV data were manually 100% *i*R compensated with R_s values acquired from the electrochemical impedance spectroscopic (EIS) analysis. EIS analysis was conducted in the frequency range of 0.1 to 1000 Hz with 5 mV amplitude at potentials where the working electrode could reach the benchmarking current density of 10 mA cm^{-2}. The potential was converted to RHE in accordance with earlier reports.[60]

General Procedure for Catalytic Hydrogenation and Hydrogenolysis Reactions. For biomass conversion we have chosen the model compounds cinnamaldehyde, 2-hydroxy-1-phenylethanone, 4-(benzyloxy)benzaldehyde, and 2-(3-methoxyphenoxy)-1-phenylethanone and deuterated solvent $CDCl_3$, purchased from Sigma-Aldrich, and these were used without any further purification. TLC plates were purchased from Merck specialties Pvt. Ltd. The NMR spectra were recorded on a Bruker Avance-400 instrument. The biomass conversions were carried out as follows. In a 20 mL pressure tube, a mixture of the starting material and catalyst $Cu_{2-x}Te$/hyd nanochains (5 or 15 wt %) were taken up in water and stirred at 80 or 135 °C under hydrogen pressure (1 or 5 bar), and stirring was continued for 18 or 24 h. The reaction progress was monitored by TLC. After completion of the reaction, ethyl acetate was added to the mixture. The aqueous phase was extracted with ethyl acetate (two to three times). Then the combined organic extracts were dried over anhydrous sodium sulfate and the solvent was removed by a rotary evaporator under reduced pressure. The crude product so obtained was purified by column chromatography using hexane/ethyl acetate as eluent. The products were well characterized by ^1H and ^{13}C NMR spectroscopic techniques.

RESULTS AND DISCUSSION

Materials Characterization. The catalyst (copper telluride nanochains and aggregates) has been well scrutinized by various characterization techniques such as PXRD, HR-TEM, FE-SEM, EDS, HAADF, BET, and XPS analysis. The crystalline nature of the two as-prepared $Cu_{2-x}Te$ materials was confirmed by powder X-ray diffraction analysis (PXRD) at a scan rate of 5°/min. The observed PXRD pattern for both samples prepared by wet-chemical (pattern a) and hydrothermal conditions (pattern b) were stacked together, as shown in Figure 1. The diffraction pattern clearly confirmed the formation of $Cu_{2-x}Te$ and matches well with the reference JCPDS file number: 00-010-0421.[61−63] The major peaks at 24.7, 27.7, 36.2, 42.9, 43.5, 45.44, 50.67, and 64.6° corresponded to the planes of (200), (106), (213), (0010), (119), (209), (401), and (1114), respectively. These planes

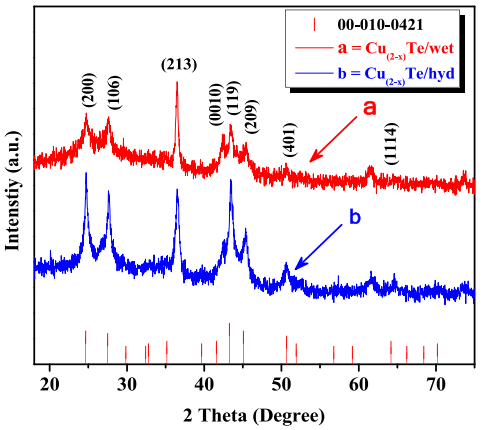

Figure 1. Stacked powder X-ray diffraction (PXRD) pattern of (a) $Cu_{2-x}Te$/wet nanoaggregates and (b) $Cu_{2-x}Te$/hyd nanochains.

were confirmed for the catalysts prepared under both wet-chemical and hydrothermal conditions. The $Cu_{2-x}Te$ catalyst shows the hexagonal crystal system with the space group *P*3*m*1, and this hexagonal system has detailed in an SAED pattern from HR-TEM images as discussed below. The crystallinity is also a factor in the performance of the HER; in order to find the crystallinity of $Cu_{2-x}Te$ from PXRD peaks, the Scherrer formula was adapted (see the Supporting Information).[20,46,64,65] From PXRD the full width at half-maximum (fwhm) of each peak was calculated for both $Cu_{2-x}Te$ catalysts, and the corresponding results are given in Tables S1 and S2 in the Supporting Information. The fwhm values of the major planes (200), (106), and (119) in the $Cu_{2-x}Te$/wet sample are 0.31, 0.26, and 0.43, respectively, which are fairly weak in comparison to the fwhm values of 0.40, 0.47, and 0.52 for $Cu_{2-x}Te$/hyd.

The peak-averaged crystallite size for $Cu_{2-x}Te$/hyd is 20.9 nm for the hydrothermally treated catalyst and 27.9 for the wet-chemical catalyst. The results show that the crystallinity increased when the sample was treated hydrothermally at 180 °C for 3 h but the sample prepared at room temperature was relatively less crystalline. After the successful formation of $Cu_{2-x}Te$ nanochains and aggregates prepared under different conditions, they were then subjected to microscopic analysis by high-resolution transmission electron microscopy (HR-TEM). The morphology of $Cu_{2-x}Te$/hyd and $Cu_{2-x}Te$/wet shows the respective nanochains and nanoaggregates (Figure 2). $Cu_{2-x}Te$/hyd shows smooth-surfaced nanochains on the nanolevel (Figure 2a,b), whereas in the case of $Cu_{2-x}Te$/wet, a morphological trend of nanoaggregates was observed, as shown in high-magnification images (Figure 2e,f).

In addition, the different magnified HR-TEM images of both the catalyst are given in Figure S1. Precise nanochains with low- and high-magnification morphological images ($Cu_{2-x}Te$/hyd) (Figure S1a,b) and nanoaggregates ($Cu_{2-x}Te$/wet) (Figure S1c,d) are observed. From high-resolution micrographs (Figure 2c,g) multiple lattice fringes was observed with *d* spacing values that correspond to the Miller indices (119), (200), and (213), respectively, for both samples. The crystal pattern obtained from HR-TEM was in perfect accordance with the PXRD pattern with ICPDS no. 00-010-0421. Figure 2d,h gives the selected area electron diffraction (SAED) patterns, which appear as main zones of large crystals that were indexed with clear spots of a hexagonal symmetry system. Along with this hexagonal system, some polycrystalline spots

https://dx.doi.org/10.1021/acs.inorgchem.0c01648
Inorg. Chem. XXXX, XXX, XXX−XXX

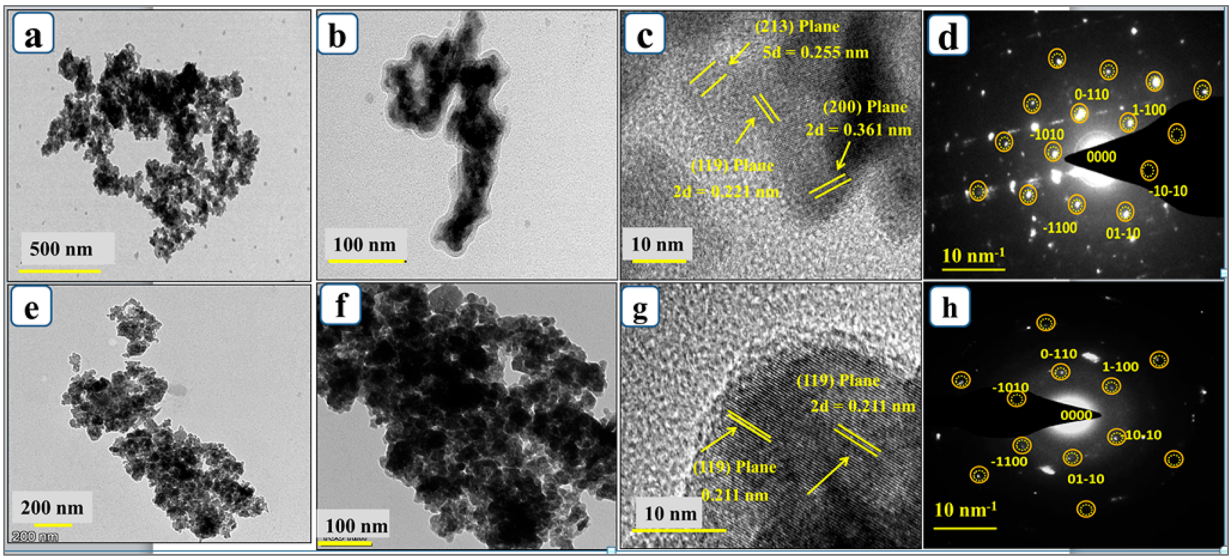

Figure 2. Low (a)- and high-magnification (b) HR-TEM images of $Cu_{2-x}Te$/hyd nanochains, low (e)- and high-magnification (f) HR-TEM images of $Cu_{2-x}Te$/wet nanoaggregates, high-magnification HR-TEM micrographs of $Cu_{2-x}Te$/hyd (c) and $Cu_{2-x}Te$/wet (g) nanochains and aggregates, the selected area electron diffraction (SAED) pattern of nanochains (d) and aggregates (h).

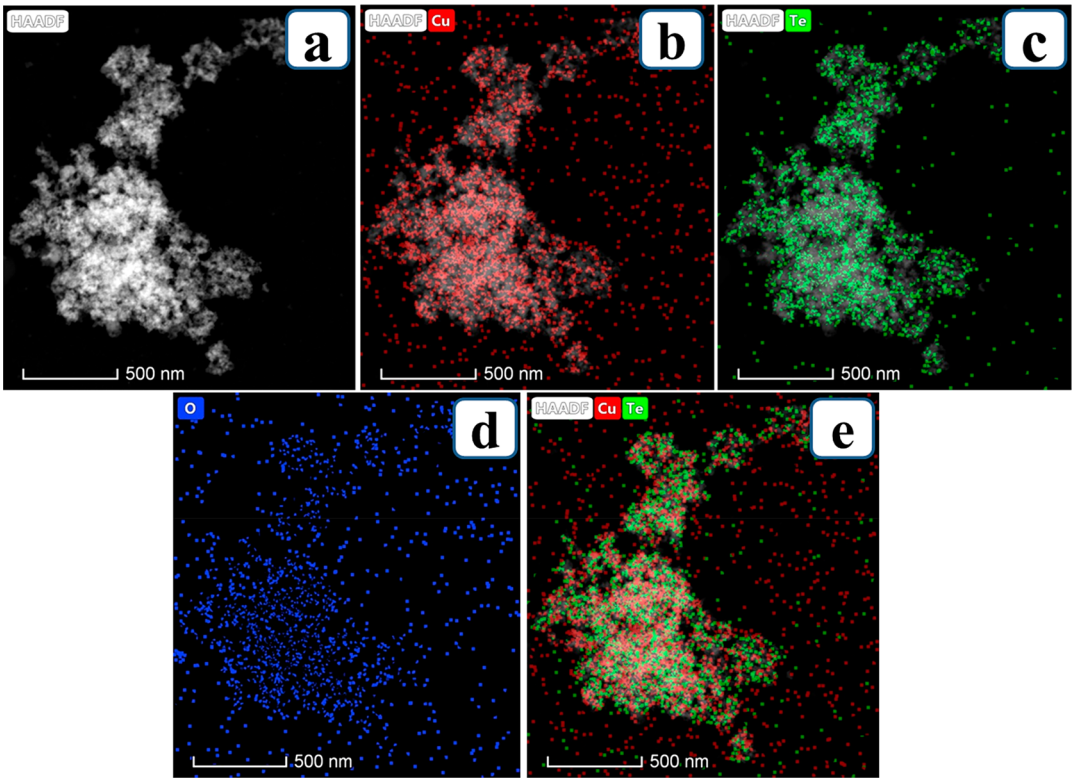

Figure 3. Low-magnification HR-TEM image of (a) $Cu_{2-x}Te$/hyd nanochains with all the elemental presence of Cu, Te, O, and N, HAADF images (b, c) HR-TEM micrographs of $Cu_{2-x}Te$/hyd nanochains containing Cu and Te, HAADF image for oxygen (d), and the overlap image (e) of evenly distributed Cu and Te.

were also observed, which might be the reason for overlapping of different domain areas (Figure 2d,h). The resulting SAED pattern is in good accordance with the PXRD file no. 010-0421.

Further, morphological analysis was carried with field emission scanning electron microscopy (FE-SEM), as shown in Figure S2. From the FE-SEM images, similar nanochain morphologies were observed for $Cu_{2-x}Te$/hyd (Figure S2a,b) and nanoaggregates for $Cu_{2-x}Te$/wet (Figure S2c,d). Also, the average particle sizes of $Cu_{2-x}Te$ in both catalysts were calculated to be ~60−80 nm. The fine morphological analysis offers a way to find the elemental presence and their composition in $Cu_{2-x}Te$. To elucidate the elemental composition, high angle annular dark field (HAADF) color mapping in the HR-TEM mode was performed (Figure 3). The low-magnification HR-TEM image area is chosen to carry

https://dx.doi.org/10.1021/acs.inorgchem.0c01648
Inorg. Chem. XXXX, XXX, XXX−XXX

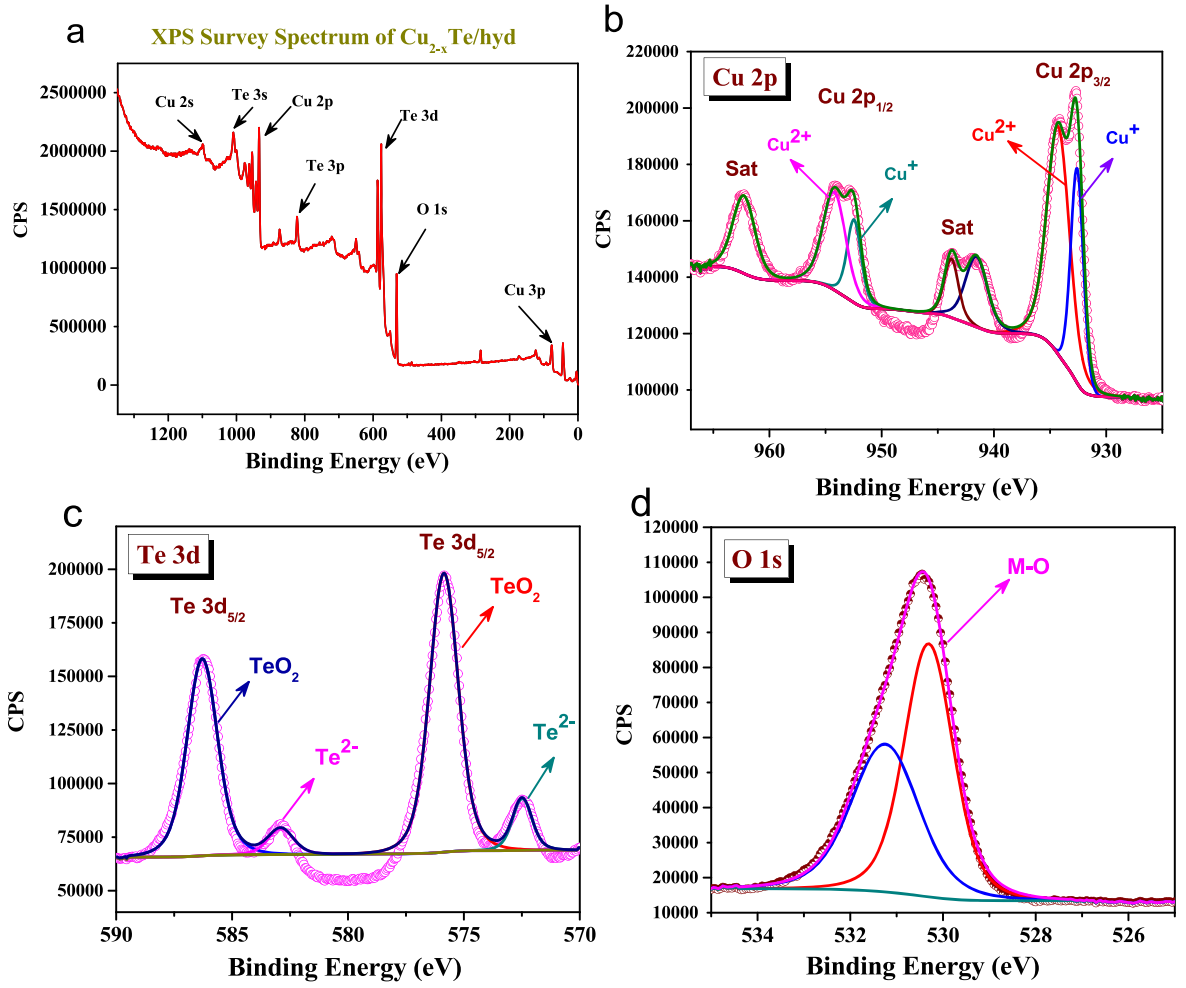

Figure 4. X-ray photoelectron spectroscopic (XPS) analysis of $Cu_{2-x}Te$/hyd nanochains: the survey spectrum (a) and high-resolution spectra of Cu 2p (b), Te 3d (c), and O 1s (d).

out the HAADF color mapping of the as-synthesized $Cu_{2-x}Te$/hyd catalyst (Figure 3a). From Figure 3a, the presence of elements such as Cu, Te, O, and C was confirmed. Figure 3b,c shows the HAADF images with a uniform distribution of copper and tellurium. Along with Cu and Te, the presence of oxygen was also observed in the color mapping, which might be due to surface oxidation (Figure 3d). The mixtures of all the elemental components are shown in HAADF mapping (Figure 3e). Further, energy dispersive X-ray spectroscopy (EDS) in the FE-SEM mode was performed for $Cu_{2-x}Te$ nanochains and aggregates and is shown in Figures S3 and S4. The resulting spectrum contains the elemental presence of Cu, Te, O, and Au. The observed EDS spectra contains no peaks for Na and Cl, which indicates the thorough washing of sample, which results the high purity of $Cu_{2-x}Te$/hyd. A similar elemental presence of Cu, Te, and O was observed for the nano-aggregates of $Cu_{2-x}Te$/wet. The presence of the Au peak is because of the Armstrong level gold sputtering. The detailed characterization results confirm the successful formation of nanochains and aggregates of $Cu_{2-x}Te$.

Further, the oxidation state of $Cu_{2-x}Te$/hyd was effectively scrutinized by an X-ray photo electron spectroscopic (XPS) study (Figure 4). Here, the overall XPS survey spectrum confirms the Cu 2p, Te 3d, and O 1s elements at their consistent binding energy values of 933.1, 572.4, and 530.1 eV, respectively (Figure 4a). Further, the high-resolution deconvoluted spectra of Cu 2p (Figure 4b) show the presence of two doublet peaks along with the corresponding satellite peaks. The spin orbital coupling of Cu $2p_{3/2}$ evidences the presence of +1 and +2 oxidation states at binding energy values of 931.8 and 932.8 eV, respectively.[66−68] The occurrence of +1 and +2 oxidation states of Cu was in perfect accordance with the PXRD results, where we have found that the oxidation state lies between +1 and +2, and a similar trend was also observed for Cu $2p_{1/2}$. Figure 4c shows the high-resolution deconvoluted spectra of Te $3d_{5/2}$, where tellurium exhibits −2 and +4 oxidation states in $Cu_{2-x}Te$ and TeO_2 at binding energies of 572.5 and 575.8 eV, respectively. Similar results were also seen with Te $3d_{3/2}$.[48] The shift in the binding energy of the O 1s spectrum (Figure 4d) evidences the M−O bond formation with either Cu or Te. The survey spectrum of $Cu_{2-x}Te$/wet confirms the presence of expected elements such as Cu, Te, and O (Figure S5a). Figure S5b gives the Cu 2p high-resolution spectrum, which reveals the presence of Cu in +1 and +2 oxidation states. Also, Te^{2-} and Te^{4+} oxidation states were observed from a Te 3d high-resolution spectrum (Figure S5c). The oxygen (O 1s) spectrum exhibits M−O interactions similar to those observed in $Cu_{2-x}Te$/hyd (Figure S5d).

The overall results confirm the copper telluride formation in the $Cu_{2-x}Te$/hyd and $Cu_{2-x}Te$/wet catalysts. After the formation of copper telluride and the morphology and chemical nature were confirmed by advanced material

https://dx.doi.org/10.1021/acs.inorgchem.0c01648
Inorg. Chem. XXXX, XXX, XXX−XXX

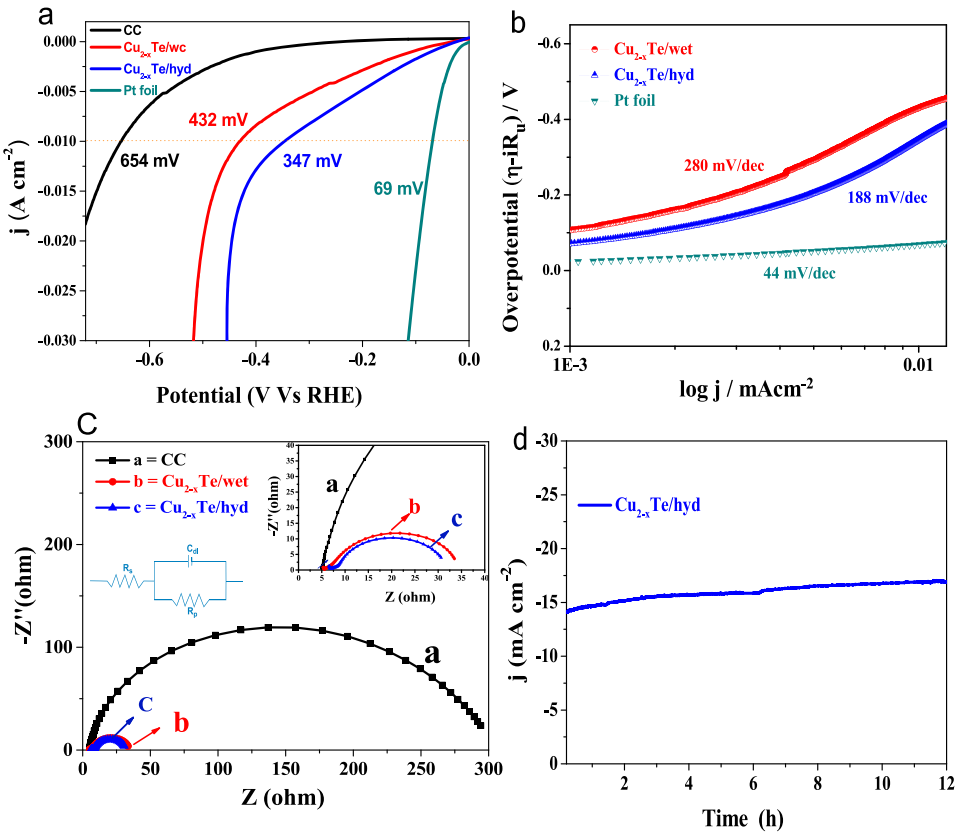

Figure 5. Linear sweep voltammetry curves of carbon cloth, $Cu_{2-x}Te$/hyd, $Cu_{2-x}Te$/wet, and Pt foil (a), Tafel analysis (b), a Nyquist plot (c), and a chronoamperometry study (d) at 10 mA cm^{-2} in 0.5 M H_2SO_4.

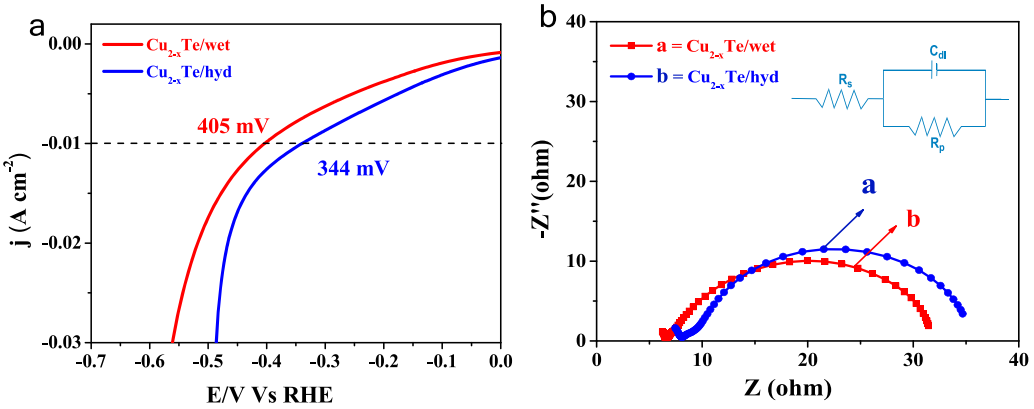

Figure 6. Linear sweep voltammetry curves (a) of $Cu_{2-x}Te$/hyd and $Cu_{2-x}Te$/wet after a long-term study and EIS analysis (b) of $Cu_{2-x}Te$/hyd and $Cu_{2-x}Te$/wet after a long-term study.

characterization techniques, the potentiality of the prepared samples were subjected for electrocatalytic HER studies under acidic conditions.

Electrocatalytic Hydrogen Evolution Reaction (HER) Studies in 0.5 M H_2SO_4. Both $Cu_{2-x}Te$/wet and $Cu_{2-x}Te$/hyd electrocatalyst have been studied for the HER in 0.5 M H_2SO_4 for the first time. Figure 5a shows the LSV of carbon cloth, $Cu_{2-x}Te$/wet, $Cu_{2-x}Te$/hyd, and Pt foil, respectively. The result from LSV shows that, to reach a current density of 10 mA cm^{-2}, interestingly $Cu_{2-x}Te$/hyd requires the lowest overpotential of 347 mV, but in the case of $Cu_{2-x}Te$/wet, it shows a higher overpotential of 432 mV (Figure 5a). The bare carbon cloth (CC) shows an overpotential of 654 mV at the same current density. The low HER overpotential of the $Cu_{2-x}Te$/hyd nanochain catalyst in comparison to the $Cu_{2-x}Te$/wet aggregates (Figure 5a) is mainly due to the creation of a greater number of active surface sites during the synthesis methodology. To get further insight into the charge transfer kinetics of the electrode/electrolyte interface of $Cu_{2-x}Te$/hyd, Tafel analysis was performed by taking the logarithm of the current density with the applied overpotential.

The hydrothermally prepared catalyst ($Cu_{2-x}Te$/hyd) displayed facile kinetics with a lower Tafel slope value of 188 mV/dec (Figure 5b). The wet chemically prepared ($Cu_{2-x}Te$/wet) catalyst showed a Tafel slope value of 280 mV/dec, which is 92 mV/dec higher than that for $Cu_{2-x}Te$/hyd. The charge transfer resistance with the electrode−electrolyte interface was determined at a potential of −380

https://dx.doi.org/10.1021/acs.inorgchem.0c01648
Inorg. Chem. XXXX, XXX, XXX−XXX

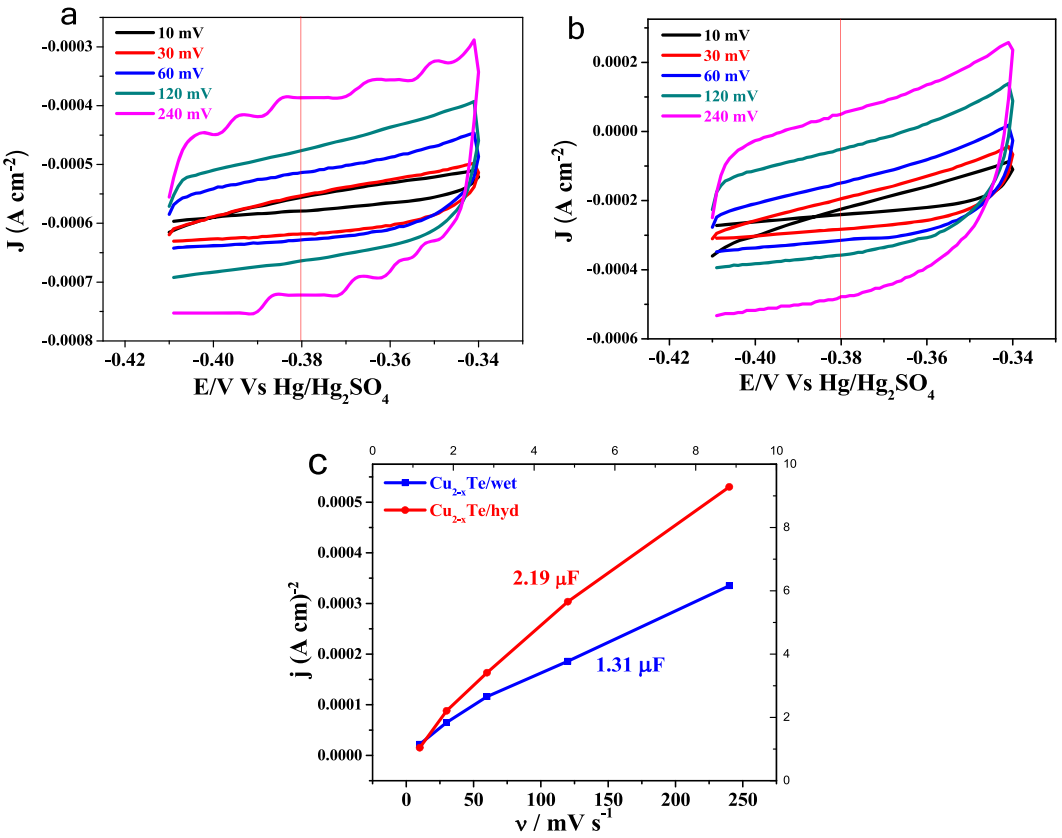

Figure 7. CV curves of $Cu_{2-x}Te$/hyd (a) and $Cu_{2-x}Te$/wet (b) determined at different scan rates from 10 to 240 mV/s to calculate the active surface area and linear plots of C_{dl} current density vs scan rate (c).

mV for all of the catalysts, and the observed trend was in exact agreement with the studies. The charge transfer resistance (R_{ct}) values of $Cu_{2-x}Te$/hyd and $Cu_{2-x}Te$/wet are 24.4 and 28.6 Ω, respectively (Figure 5c), which is in accordance with the LSV results observed. The bare CC showed a higher R_{ct} value of 300 Ω in comparison to the catalysts, indicating the poor inherent charge transfer. To get an insight into the tellurides of Cu under acidic conditions, a stability study was carried out by a chronoamperometry for 12 h, and result is depicted in Figure 5d. The activity was retained even after 12 h of continuous static potential. The same was evidenced from the potentiodynamic conditions, where a cycling study was carried out for 250 cycles at a scan rate of 100 mV/s for both catalysts. The electrocatalytic activity at a current density of 10 mA cm^{-2} was monitored after 250 cycles and is represented in Figure 6a.

The HER activity is stable enough even after 250 cycles; no change in current was observed (Figure 6a), and overpotentials of 344 and 405 mV were obtained for $Cu_{2-x}Te$/hyd and $Cu_{2-x}Te$/wet, respectively (Figure 6a). Moreover, the small change in R_{ct} values indicated the higher stability of $Cu_{2-x}Te$/hyd and $Cu_{2-x}Te$/wet under harsh acidic conditions (Figure 6b). ECSA has been chosen as a method to find the cause of dissimilarities during the comparison of electrocatalytic activity among the similar catalytic materials.[59] To determine the active surface area of these two catalysts, the electrochemical surface area (ECSA) has been measured from the double-layer capacitance values (C_{dl}), which are shown in Figure 7.

Figure 7a,b shows the CV responses of $Cu_{2-x}Te$-wet and $Cu_{2-x}Te$-hyd in 0.5 M H_2SO_4 with different scan rates of 10, 30, 60, 120, and 240 mV/s. The slope from current vs scan rate showed a linear increment with a slope of 2.19 μF for $Cu_{2-x}Te$-hyd, which is found to be superior in comparison to $Cu_{2-x}Te$-wet, which actually showed 1.31 μF (Figure 7c). A Brunauer–Emmett–Teller (BET) analysis was performed to determine the surface areas of both catalysts. The observed surface areas were 22.3 m^2/g for $Cu_{2-x}Te$-hyd and 21.9 m^2/g for $Cu_{2-x}Te$-wet sample, respectively (Figure S6). The pore size was observed to be 0.112 cm^3/g for $Cu_{2-x}Te$-hyd. The turnover frequencies (TOF) were calculated for both catalysts using the formula TOF = $jA/2Fm$[59,68] and is discussed in detail in the Supporting Information. Moreover, the Faradaic efficiency was calculated for $Cu_{2-x}Te$/hyd by collecting H_2 gas from the electrochemical cell and measured by gas chromatography. The calculated Faradaic efficiency was around 95.06% (Figure S7). These findings clearly portray that the prepared catalysts acted as high-performance catalysts in the HER in acidic medium. We have compared our $Cu_{2-x}Te$-hyd catalyst with other copper-based and tellurium-based materials utilized for the HER, and the results are given in Tables S3 and S4 in the Supporting Information. These kinds of less explored Cu-based tellurides will be of highly useful for other energy related applications.

Catalytic Hydrogenation/Hydrogenolysis of a Feedstock Model Compound. Towards the idea of utilizing hydrogen produced from electrocatalytic water splitting by the novel catalyst $Cu_{2-x}Te$/hyd nanochains in real-life applications, the conversion of agricultural waste to value-added products has been demonstrated (Scheme 1a). In biomass constituents two functional groups are present in large quantity, such as ether linkages and carbonyls derived from alcohols. Along this line we have chosen biomass model

https://dx.doi.org/10.1021/acs.inorgchem.0c01648
Inorg. Chem. XXXX, XXX, XXX−XXX

Scheme 1. Representative Structure of Feedstock Material (Lignin) (a) and Catalytic Hydrogenation (b) and Hydrogenolysis of Feedstock Mimics on a Large Scale (c)

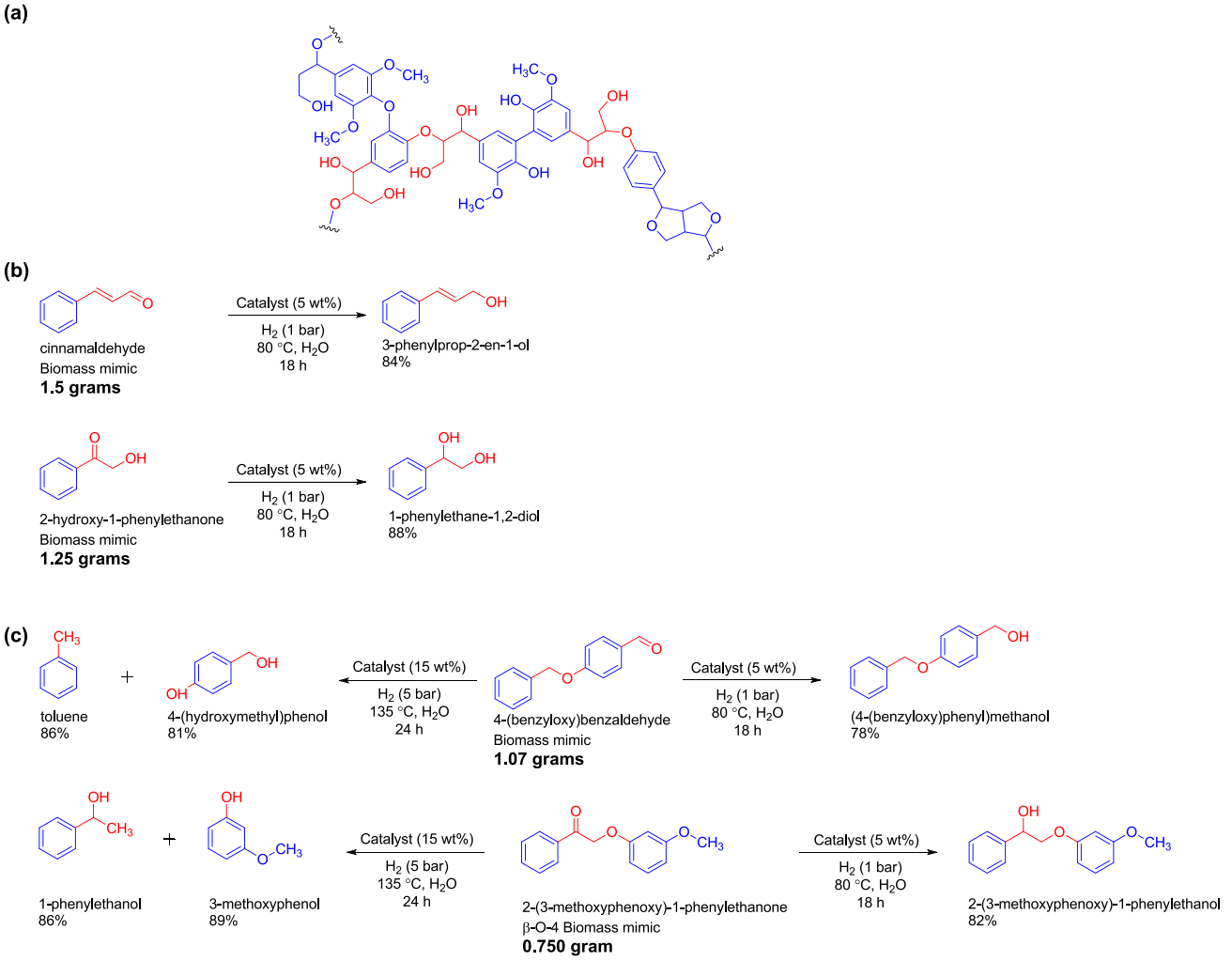

compounds containing benzylic alcohols and ether linkages, which are converted to the corresponding hydrogenated and hydrogenolyzed products in aqueous medium. The optimization reaction was performed by taking 4-(benzyloxy)-benzaldehyde as a feedstock model compound for both hydrogenation and hydrogenolysis reactions. We found that 0.75 mmol of the starting material was successfully converted to the corresponding (4-(benzyloxy)phenyl)methanol by a hydrogenation reaction using 5 wt % of catalyst in 1.0 mL of water at 80 °C for 18 h (Table S5 in the Supporting Information).

4-Benzyloxybenzaldehyde was efficiently converted to the respective 4-(hydroxymethyl)phenol and toluene by a hydrogenolysis reaction using 15 wt % of catalyst in 1.0 mL of water at 135 °C for 24 h (Table S6 in the Supporting Information). These results encouraged us to carry out the conversion of other feedstock mimics under the optimized conditions. Taking advantage of the optimized conditions, we have performed hydrogenation reactions using cinnamaldehyde and 2-hydroxy-1-phenylethanone as feedstock model compounds on a large scale and the respective yields are given in Scheme 1b. Also, we extended this protocol to both hydrogenation and hydrogenolysis reactions by taking 4-benzyloxybenzaldehyde and 2-(3-methoxyphenoxy)-1-phenylethanone as feedstock motifs on a large scale and the yields are given in Scheme 1c. The obtained products were separated by column chromatography using ethyl acetate−hexane as the eluent, and the purities of the compounds were confirmed by NMR spectroscopy (Figures S8−S23). The corresponding photographic image of large-scale reactions is given in Figure S24.

Moreover, the conversion of feedstock materials to different value-added products by simply changing the reaction conditions under hydrogen pressure in aqueous medium is scarce in the literature. We have compared the advantages of $Cu_{2-x}Te$/hyd with other reported catalysts, as given in Table S7, and also with other various Cu-based catalysts, as given in Table S8 in the Supporting Information. These aforementioned reactions proved the ability of the developed catalyst $Cu_{2-x}Te$/hyd toward feedstock conversion on a large scale for industrial processes.

Further, recyclability experiments were carried out up to eight cycles using a simple "in-flask" workup for the hydrogenation reaction by using a 3.75 mmol scale of the aldehyde under the optimized conditions and kinetically controlled regime for 4 h (Figure 8) (see the Supporting Information). After each cycle, we observed good yields, which shows the robustness of the developed catalyst. The conversion

https://dx.doi.org/10.1021/acs.inorgchem.0c01648
Inorg. Chem. XXXX, XXX, XXX−XXX

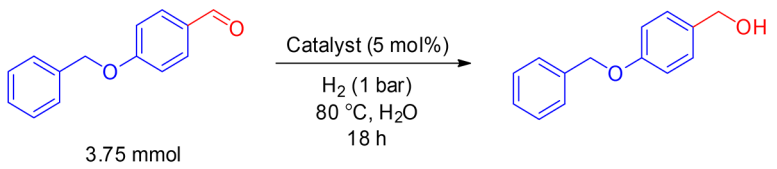

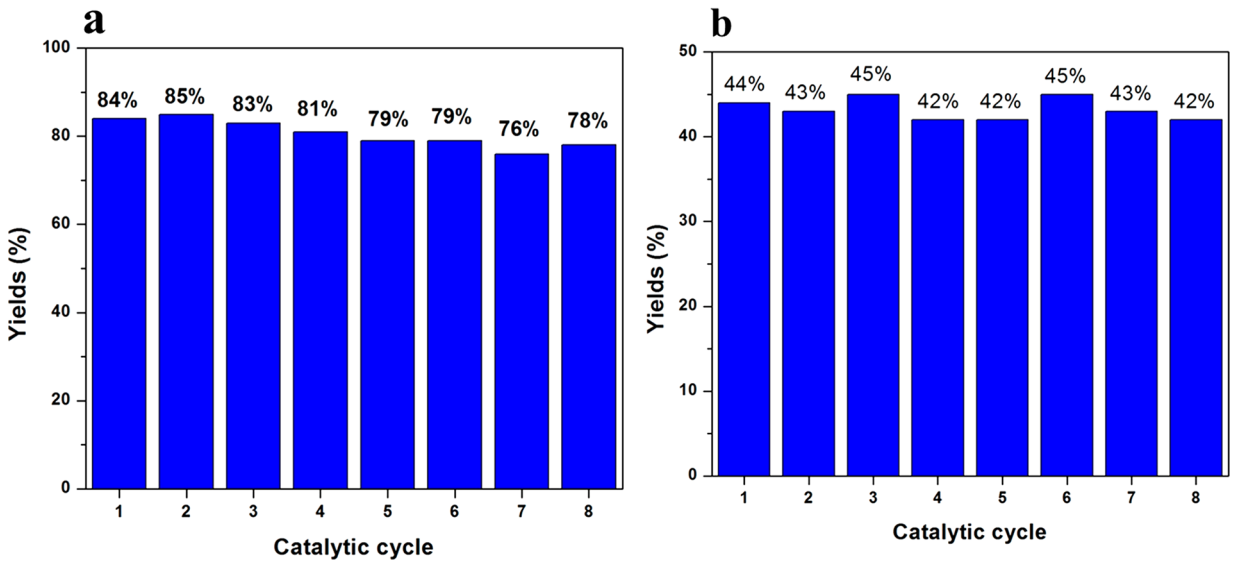

Figure 8. Recyclability for hydrogenation of 4-(benzyloxy)benzaldehyde under (a) optimized conditions and (b) the kinetically controlled regime for 4 h.

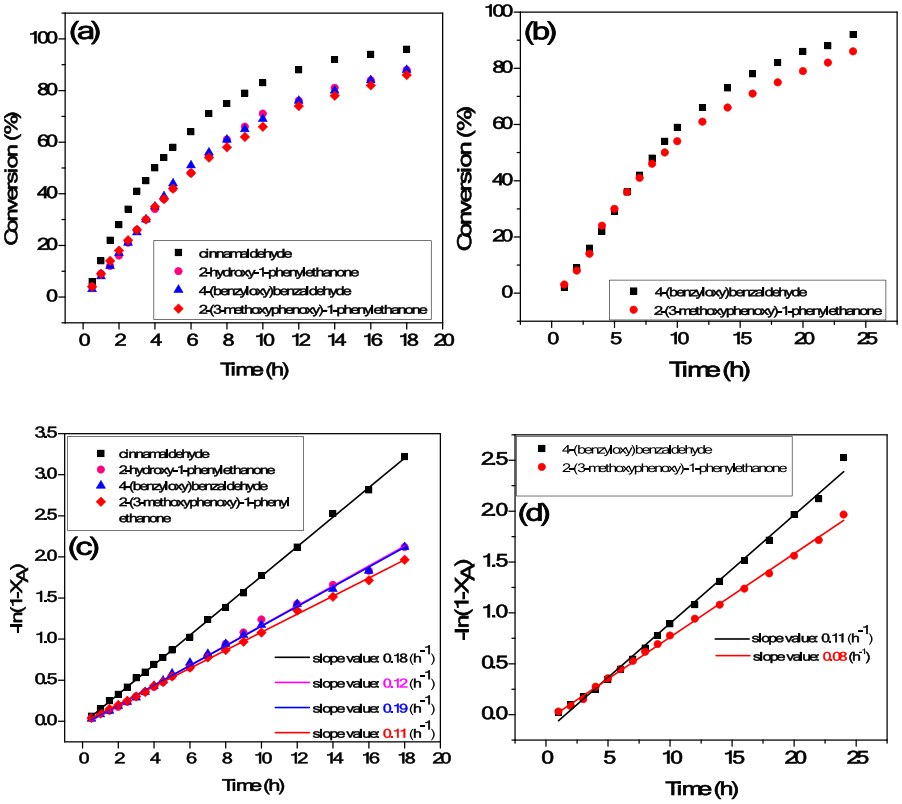

Figure 9. (a, c) Conversions of hydrogenation and hydrogenolysis of carbonyls, respectively, and (b, d) rate constants for hydrogenation and hydrogenolysis of carbonyls, respectively.

of biomass aldehyde with respect to time (h) shows second-order rate kinetics, and the rate constants (k) were found to be 0.36, 0.24, 0.38, and 0.22 L mol^{-1} h^{-1} for hydrogenation of the feedstock model compounds cinnamaldehyde, 2-hydroxy-1-

https://dx.doi.org/10.1021/acs.inorgchem.0c01648
Inorg. Chem. XXXX, XXX, XXX−XXX

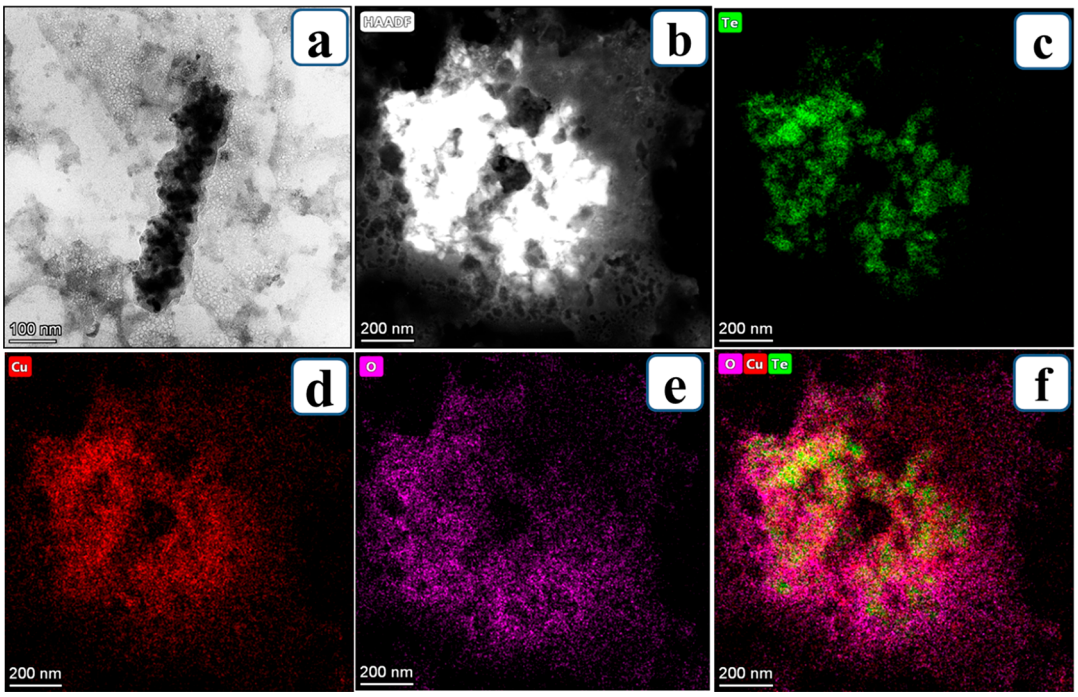

Figure 10. (a) Post high resolution HR-TEM image of $Cu_{2-x}Te$/hyd nanochains, (b) the HR-TEM image chosen for HAADF mapping, (c−e) the corresponding individual HAADF maps of Te, Cu, and O and (f) the overlapped HAADF mapping of Te, Cu, and O together.

phenylethanone, 4-(benzyloxy)benzaldehyde, and 2-(3-methoxyphenoxy)-1-phenylethanone, respectively. Along the same line the rate constants (k) were found to be 0.22 and 0.16 L mol^{-1} h^{-1} for hydrogenolysis of 4-(benzyloxy)-benzaldehyde and 2-(3-methoxyphenoxy)-1-phenylethanone, respectively (Figure 9).

Post-HER Morphological and Elemental Studies of $Cu_{2-x}Te$/hyd Nanoaggregates. The electrochemical HER performances of both $Cu_{2-x}Te$/wet and $Cu_{2-x}Te$/hyd were well studied in 0.5 M H_2SO_4. After this, post characterizations were performed for the best sample $Cu_{2-x}Te$/hyd nanochains to identify the morphological and elemental changes in the sample after the HER studies. At first, a post morphological study was carried out by HR-TEM, which exhibits nanochains similar to those in Figure 2a. A high-magnification HR-TEM image after the HER is shown in Figure 10a, where we can see the stable nanochain morphology is retained with slight agglomeration. This agglomeration is mainly due to the sonication of the sample to peel it off from the carbon cloth after the HER study. Some addititonal HR-TEM images are provided in Figure S25a,b, which confirmed the nanochain morphology of $Cu_{2-x}Te$/hyd after the HER studies.

Also, similar crystal lattice fringes were observed for $Cu_{2-x}Te$/hyd nanochains, as shown in Figure S25c. The post selected area diffraction image showed the polycrystalline nature and matched with the (119) plane, in accordance with the PXRD reference JCPDS file number 00-010-0421 (Figure S25d). The stability and robustness for of the novel $Cu_{2-x}Te$/hyd nanoaggregate electrocatalyst were further scrutinized in HAADF color mapping and EDS analysis. Figure 10b gives an HR-TEM image chosen to scan the elemental presence, especially Te, in the $Cu_{2-x}Te$/hyd after the HER studies via HAADF color mapping, and the results can be visualized by the uniform distribution of copper, tellurium, and oxygen, proving the stable nature (Figure 10c−f). The individual screening of the elemental presence of Te and Cu in the sample also confirmed the stability of the catalyst after a long-term HER study. In addition to color mapping, the post EDS analysis is also a proof to support the stability of the catalyst ($Cu_{2-x}Te$/hyd) after the HER study.

The similar elemental presence coincides with that of EDS before the HER analysis, as depicted in Figure S26 in the Supporting Information. After this, the chemical nature was further verified with an XPS analysis and is shown in Figure S27 in the Supporting Information. The oxidation states of Cu were found to be +1 and +2 from Figure S27a and the −2 and +4 oxidation states of Te from Figure S27b. This shows the extremely stable nature of Cu and Te even after the HER responses. The O 1s spectrum from Figure S27c shows the presence of surface oxides, as observed in Figure 4. A post XRD analysis was carried after the electrochemical HER studies, and it showed no diffraction pattern (Figure S28 in the Supporting Information). This is because after a long-term stability study the catalytic surface would have been less pronounced (0.2 mg cm^{-2} of catalyst for HER study) for the incident X-ray beam. Hence, the scattering hardly observed much instead we obtained peaks only for the substrate carbon cloth used. From the overall post characterization study, we conclude that $Cu_{2-x}Te$/hyd is highly stable after the HER under acidic conditions. Therefore, modification of the underutilized copper can change it from an inactive, higher overvoltage electrocatalyst to a superior catalyst for HER analysis.

CONCLUSION

Here, we have developed an earth-abundant and cost-effective novel electrocatalyst, copper telluride ($Cu_{2-x}Te$) nanochains and aggregates, for the hydrogen evolution reaction. The overvoltage when pure copper metal is used was effectively reduced by the successful tellurization of copper via different synthetic methodologies such as hydrothermal and wet-chemical routes. During the HER, in order to gain a current

https://dx.doi.org/10.1021/acs.inorgchem.0c01648
Inorg. Chem. XXXX, XXX, XXX−XXX

density of 10 mA cm^{-2}, $Cu_{2-x}Te$/hyd exhibited a very low overpotential of 347 mV. Also, $Cu_{2-x}Te$/hyd showed a very low R_{ct} value of 24.4 Ω. The chronoamperometry study shows the highly stable nature of the $Cu_{2-x}Te$/hyd catalyst over prolonged exposure 0.5 M H_2SO_4. The Faradaic efficiency value for $Cu_{2-x}Te$/hyd catalyst was found to be 95.06%. Post studies confirmed the stable nature of the $Cu_{2-x}Te$ catalysts. Notably, for the first time in the literature, the idea of utilizing hydrogen evolved from water electrolysis has been successfully demonstrated for the feedstock conversion to fine chemical synthesis via hydrogenation and hydrogenolysis processes under external hydrogen pressure. An environmentally green, large-scale production of fine chemicals proves the industrial applicability of the $Cu_{2-x}Te$/hyd nanochain catalyst. In addition, the satisfactory recyclability results prove the robustness of the developed catalyst. Moreover, the preparation of the catalyst, water electrolysis, and feedstock conversions have been demonstrated in aqueous medium under mild conditions, which offers an environmentally friendly green protocol for fuel generation and platform chemical synthesis. Therefore, the developed catalyst offers a great advantage to design a cost-effective and stable electrocatalyst in real-life application in the coming years. In addition, the direct utilization of hydrogen produced from electrocatalytic water splitting to feedstock conversion for fine chemical synthesis can also be a practical application in the near future. In a continuation of these findings, the water electrolysis under flow reactor conditions followed by utilization of in situ generated H_2 in feedstock conversion for industrial applicability is in progress in our laboratory.

■ ASSOCIATED CONTENT

Supporting Information

The Supporting Information is available free of charge at https://pubs.acs.org/doi/10.1021/acs.inorgchem.0c01648.

Materials and characterization techniques, information on crystallinity calculations, optimization of the feedstock conversion, a comparison table, a synthesis scheme, and figures related to $Cu_{2-x}Te$ (PDF)

■ AUTHOR INFORMATION

Corresponding Author

Subrata Kundu − *Materials Electrochemistry Division (MED), CSIR-Central Electrochemical Research Institute (CECRI), Karaikudi 630003, Tamil Nadu, India; Academy of Scientific and Innovative Research (AcSIR), Ghazizbad 201002, India;* orcid.org/0000-0002-1992-9659; Phone: +91 4565-241487; Email: skundu@cecri.res.in, kundu.subrata@gmail.com

Authors

Sangeetha Kumaravel − *Materials Electrochemistry Division (MED), CSIR-Central Electrochemical Research Institute (CECRI), Karaikudi 630003, Tamil Nadu, India; Academy of Scientific and Innovative Research (AcSIR), Ghazizbad 201002, India;* orcid.org/0000-0001-5044-6084

Kannimuthu Karthick − *Materials Electrochemistry Division (MED), CSIR-Central Electrochemical Research Institute (CECRI), Karaikudi 630003, Tamil Nadu, India; Academy of Scientific and Innovative Research (AcSIR), Ghazizbad 201002, India;* orcid.org/0000-0003-2689-0657

Prabaharan Thiruvengetam − *Department of Chemistry, Indian Institute of Technology Madras, Chennai 600036, India*

Jinta Merlin Johny − *Materials Electrochemistry Division (MED), CSIR-Central Electrochemical Research Institute (CECRI), Karaikudi 630003, Tamil Nadu, India*

Selvasundarasekar Sam Sankar − *Materials Electrochemistry Division (MED), CSIR-Central Electrochemical Research Institute (CECRI), Karaikudi 630003, Tamil Nadu, India; Academy of Scientific and Innovative Research (AcSIR), Ghazizbad 201002, India;* orcid.org/0000-0003-2262-7739

Complete contact information is available at: https://pubs.acs.org/10.1021/acs.inorgchem.0c01648

Notes

The authors declare no competing financial interest.

■ ACKNOWLEDGMENTS

We wish to acknowledge Dr. N. Kalaiselvi, Director, CSIR-CECRI, for her continuous support and encouragement. S.K. wishes to acknowledge the DST (Department of Science and Technology), New Delhi, for an Inspire fellowship. K.K. and S.S.S. wish to acknowledge the UGC (University Grants Commission) for research fellowships, respectively. All of the authors wish to acknowledge the central instrumental facility (CIF), CSIR-CECRI, for its full-time support. S.K. acknowledges the Department of Science and Technology (DST) for EMR research funding by # EMR/2017/000860 on May 11th, 2018, with institute OM number 18-29-03/(27/2018)-TTBD-CSIR-CECRI on October 29, 2018.

■ REFERENCES

(1) Habas, S. E.; Platt, H. A. S.; van Hest, M. F. A. M.; Ginley, D. S. Low-Cost Inorganic Solar Cells : From Ink To Printed Device. *Chem. Rev.* **2010**, *110*, 6571−6594.

(2) Dresselhaus, M. S.; Thomas, I. L. Alternative Energy Technologies. *Nature* **2001**, *414*, 332−337.

(3) Hisatomi, T.; Kubota, J.; Domen, K. Recent Advances in Semiconductors for Photocatalytic and Photoelectrochemical Water Splitting. *Chem. Soc. Rev.* **2014**, *43*, 7520−7535.

(4) Jin, H.; Guo, C.; Liu, X.; Liu, J.; Vasileff, A.; Jiao, Y.; Zheng, Y.; Qiao, S. Emerging Two-Dimensional Nanomaterials for Electrocatalysis. *Chem. Rev.* **2018**, *118*, 6337−6408.

(5) Turner, J. A. Sustainable Hydrogen Production. *Science* **2004**, *305*, 972−974.

(6) Chen, H. M.; Chen, K.; Liu, R.; Zhang, L.; Zhanng, J.; Wilkinson, D. P. Nano-Architecture and Material Designs for Water Splitting Photoelectrodes. *Chem. Soc. Rev.* **2012**, *41*, 5654−5671.

(7) Walter, M. G.; Warren, E. L.; Mckone, J. R.; Boettcher, S. W.; Mi, Q.; Santori, E. A.; Lewis, N. S. Solar Water Splitting Cells. *Chem. Rev.* **2010**, *110*, 6446−6473.

(8) Gao, M.; Liang, J.; Zheng, Y.; Xu, Y.; Jiang, J.; Gao, Q.; Li, J.; Yu, S. An Efficient Molybdenum Disulfide/Cobalt Diselenide Hybrid Catalyst for Electrochemical Hydrogen Generation. *Nat. Commun.* **2015**, *6*, 5982.

(9) Yu, Y.; Shi, Y.; Zhang, B. Synergetic Transformation of Solid Inorganic − Organic Hybrids into Advanced Nanomaterials for Catalytic Water Splitting. *Acc. Chem. Res.* **2018**, *51*, 1711−1721.

(10) Mueller-langer, F.; Tzimas, E.; Kaltschmitt, M.; Peteves, S. Techno-Economic Assessment of Hydrogen Production Processes for the Hydrogen Economy for the Short and Medium Term. *Int. J. Hydrogen Energy* **2007**, *32*, 3797−3810.

(11) Anantharaj, S.; Ede, S. R.; Sakthikumar, K.; Karthick, K.; Mishra, S.; Kundu, S. Recent Trends and Perspectives in Electrochemical Water Splitting with an Emphasis on Sulfide, Selenide, and

https://dx.doi.org/10.1021/acs.inorgchem.0c01648
Inorg. Chem. XXXX, XXX, XXX−XXX

Phosphide Catalysts of Fe, Co, and Ni: A Review. *ACS Catal.* **2016**, *6*, 8069−8097.
(12) Menezes, P. W.; Indra, A.; Das, C.; Walter, C.; Gobel, C.; Gutkin, V.; Schmei, D.; Driess, M. Uncovering the Nature of Active Species of Nickel Phosphide Catalysts in High-Performance Electrochemical Overall Water Splitting. *ACS Catal.* **2017**, *7*, 103−109.
(13) Stamenkovic, V. R.; Mun, B. S.; Arenz, M.; Mayrhofer, K. J. J.; Lucas, C. A.; Wang, G.; Ross, P. N.; Markovic, N. M. Trends in Electrocatalysis on Extended and Nanoscale Pt-Bimetallic Alloy Surfaces. *Nat. Mater.* **2007**, *6*, 241−247.
(14) Lee, Y.; Suntivich, J.; May, K. J.; Perry, E. E.; Shao-horn, Y. Synthesis and Activities of Rutile IrO_2 and RuO_2 Nanoparticles for Oxygen Evolution in Acid and Alkaline Solutions. *J. Phys. Chem. Lett.* **2012**, *3*, 399−404.
(15) Shi, S. Y.; Zhang, B. Recent Advances in Transition Metal Phosphide Nanomaterials: Synthesis and Applications in Hydrogen Evolution Reaction. *Chem. Soc. Rev.* **2016**, *45*, 1529−1541.
(16) Kotz, R.; Stucki, S. Stabilization of RuO_2 by IrO_2 for Anodic Oxygen Evolution in Acid Medium. *Electrochim. Acta* **1986**, *31*, 1311−1316.
(17) Anantharaj, S.; Karthick, K.; Kundu, S. $NiTe_2$ Nanowire Outperforms Pt/C in High-Rate Hydrogen Evolution at Extreme pH Conditions. *Inorg. Chem.* **2018**, *57*, 3082−3096.
(18) Song, C.; Zhao, Z.; Sun, X.; Zhou, Y.; Wang, Y.; Wang, D. In Situ Growth of Ag Nanodots Decorated Cu_2O Porous Nanobelts Networks on Copper Foam for Efficient HER Electrocatalysis. *Small* **2019**, *15*, 1804268.
(19) Wu, R.; Zhang, J.; Shi, Y.; Liu, D.; Zhang, B. Metallic WO_2−Carbon Mesoporous Nanowires as Highly Efficient Electrocatalysts for Hydrogen Evolution Reaction. *J. Am. Chem. Soc.* **2015**, *137*, 6983−6986.
(20) Yan, X.; Tian, L.; Chen, X. Crystalline/Amorphous Ni/ NiO Core /Shell Nanosheets as Highly Active Electrocatalysts for Hydrogen Evolution Reaction. *J. Power Sources* **2015**, *300*, 336−343.
(21) Chen, Y.; Zhang, J.; Wan, L.; Hu, W.; Liu, L.; Zhong, C.; Deng, Y. Effect of Nickel Phosphide Nanoparticles Crystallization on Hydrogen Evolution Reaction Catalytic Performance. *Trans. Nonferrous Met. Soc. China* **2017**, *27*, 369−376.
(22) Karthick, K.; Anantharaj, S.; Patchaiammal, S.; Jagadeesan, S. N.; Kumar, P.; Ede, S. R.; Pattanayak, D. K.; Kundu, S. Advanced Cu_3Sn and Selenized Cu_3Sn@Cu Foam as Electrocatalysts for Water Oxidation under Alkaline and Near-Neutral Conditions. *Inorg. Chem.* **2019**, *58*, 9490−9499.
(23) Tran, D. T.; Le, H. T.; Luyen Doan, T. L.; Kim, N. H.; Lee, J. H. Pt Nanodots Monolayer Modified Mesoporous Cu@Cu_xO Nanowires for Improved Overall Water Splitting Reactivity. *Nano Energy* **2019**, *59*, 216−228.
(24) Anantharaj, S.; Amarnath, T. S.; Subhashini, E.; Chatterjee, S.; Swaathini, K. C. S.; Karthick, K.; Kundu, S. Shrinking the Hydrogen Overpotential of Cu by 1 V and Imparting Ultralow Charge Transfer Resistance for Enhanced H_2 Evolution. *ACS Catal.* **2018**, *8*, 5686−5697.
(25) Ye, R.; Lin, L.; Li, Q.; Zhou, Z.; Wang, T.; Russell, C. K.; Adidharma, H.; Xu, Z.; Yao, Y.-G.; Fan, M. Recent Progress in Improving the Stability of Copper-Based Catalysts for Hydrogenation of Carbon−Oxygen Bonds. *Catal. Sci. Technol.* **2018**, *8*, 3428−3449.
(26) Hou, Y.; Lohe, M. R.; Zhang, J.; Liu, S.; Zhuang, X.; Feng, X. Vertically Oriented Cobalt Selenide/NiFe Layered- Double-Hydroxide Nanosheets Supported on Exfoliated Graphene Foil: An Efficient 3D Electrode for Overall Water Splitting. *Energy Environ. Sci.* **2016**, *9*, 478−483.
(27) Dutta, S.; Indra, A.; Feng, Y.; Song, T.; Paik, U. Self-Supported Nickel Iron Layered Double Hydroxide-Nickel Selenide Electrocatalyst for Superior Water Splitting Activity. *ACS Appl. Mater. Interfaces* **2017**, *9*, 33766−33774.
(28) Trotochaud, L.; Young, S. L.; Ranney, J. K.; Boettcher, S. W. Nickel−Iron Oxyhydroxide Oxygen-Evolution Electrocatalysts : The Role of Intentional and Incidental Iron Incorporation. *J. Am. Chem. Soc.* **2014**, *136*, 6744−6753.
(29) Mathankumar, M.; Anantharaj, S.; Nandakumar, A. K.; Kundu; Subramanian, B. Potentiostatic Phase Formation of β-CoOOH on Pulsed LASER Deposited Biphasic Cobalt Oxide Thin Film for Enhanced Oxygen Evolution. *J. Mater. Chem. A* **2017**, *5*, 23053−23066.
(30) Karthick, K.; Anantharaj, S.; Karthik, P. E.; Subramanian, B.; Kundu, S. Self-Assembled Molecular Hybrids of CoS-DNA for Enhanced Water Oxidation with Low Cobalt Content. *Inorg. Chem.* **2017**, *56*, 6734−6745.
(31) Feng, Y.; Yu, X.; Paik, U. Formation of Co_3O_4 Microframes from MOFs with Enhanced Electrochemical Performance for Lithium Storage and Water Oxidation. *Chem. Commun.* **2016**, *52*, 6269−6272.
(32) Xia, C.; Liang, H.; Zhu, J.; Schwingenschlogl, U.; Alshareef, H. N. Active Edge Sites Engineering in Nickel Cobalt Selenide Solid Solutions for Highly Efficient Hydrogen Evolution. *Adv. Energy Mater.* **2017**, *7*, 1602089.
(33) Michalsky, R.; Zhang, Y.; Peterson, A. A. Trends in the Hydrogen Evolution Activity of Metal Carbide Catalysts. *ACS Catal.* **2014**, *4*, 1274−1278.
(34) Seitz, L. C.; Dickens, C. F.; Nishio, K.; Hikita, Y.; Montoya, J.; Doyle, A.; Kirk, C.; Vojvodic, A.; Hwang, H. Y.; Norskov, J. K.; Jaramillo, T. F. A Highly Active and Stable IrO_x/$SrIrO_3$ Catalyst for the Oxygen Evolution Reaction. *Science* **2016**, *353*, 1011−1014.
(35) Cobo, S.; Heidkamp, J.; Jacques, P.; Fize, J.; Fourmond, V.; Guetaz, L.; Jousselme, B.; Ivanova, V.; Dau, H.; Palacin, S.; Fontecave, M. A Janus Cobalt-Based Catalytic Material for Electro-Splitting of Water. *Nat. Mater.* **2012**, *11*, 802−807.
(36) Kumaravel, S.; Thiruvengetam, P.; Ede, S. R.; Karthick, K.; Anantharaj, S.; Sankar, S. S.; Kundu, S. Cobalt Tungsten Oxide Hydroxide Hydrate (CTOHH) on DNA Scaffold: An Excellent Bi-Functional Catalyst for Oxygen Evolution Reaction (OER) and Aromatic Alcohol Oxidation. *Dalt. Trans.* **2019**, *48*, 17117−17131.
(37) Xiao, P.; Chen, W.; Wang, X. A Review of Phosphide-Based Materials for Electrocatalytic Hydrogen Evolution. *Adv. Energy Mater.* **2015**, *5*, 1500985.
(38) Chen, W.; Schneider, J. M.; Sasaki, K.; Wang, C.; Schneider, J.; Lyer, S.; Lyer, S.; Zhu, Y.; Muckerman, J. T.; Fukjita, E. Tungsten Carbide − Nitride on Graphene Nanoplatelets as a Durable Hydrogen Evolution Electrocatalyst. *ChemSusChem* **2014**, *7*, 2414−2418.
(39) Yan, H.; Tian, C.; Wang, L.; Wu, A.; Meng, M.; Zhao, L.; Fu, H. Phosphorus-Modified Tungsten Nitride/Reduced Graphene Oxide as a High-Performance, Non-Noble-Metal Electrocatalyst for the Hydrogen Evolution Reaction. *Angew. Chem.* **2015**, *127*, 6423−6427.
(40) Kim, S. ki; Qiu, Y.; Zhang, Y.-J.; Hurt, R.; Peterson, A. Nanocomposites of Transition-Metal Carbides on Reduced Graphite Oxide as Catalysts for the Hydrogen Evolution Reaction. *Appl. Catal., B* **2018**, *235*, 36−44.
(41) Kuang, Q.; Wang, X.; Jiang, Z.; Xie, Z.; Zheng, L. High-Energy-Surface Engineered Metal Oxide Micro- and Nanocrystallites and Their Applications. *Acc. Chem. Res.* **2014**, *47* (2), 308−318.
(42) Huang, C.; Huang, Y.; Liu, C.; Yu, Y.; Zhang, B. Integrating Hydrogen Production with Aqueous Selective Semi-Dehydrogenation of Tetrahydroisoquinolines over a Ni_2P Bifunctional Electrode. *Angew. Chem., Int. Ed.* **2019**, *58*, 12014−12017.
(43) Zou, H.; Yuan, C.; Zou, H.; Cheang, T.; Zhao, S.; Qazi, U. Y.; Zhong, S.; Wang, L.; Xu, A. Bimetallic Phosphide Hollow Nanocubes Derived from a Prussian-Blue-Analog Used as High- Performance Catalysts for the Oxygen Evolution Reaction. *Catal. Sci. Technol.* **2017**, *7*, 1549−1555.
(44) Anantharaj, S.; Karthick, K.; Venkatesh, M.; Simha, T. V. S. V; Salunke, A. S.; Ma, L.; Liang, H.; Kundu, S. Enhancing Electrocatalytic Total Water Splitting at Few Layer Pt-NiFe Layered Double Hydroxide Interfaces. *Nano Energy* **2017**, *39*, 30−43.
(45) Voiry, D.; Yamaguchi, H.; Li, J.; Silva, R.; Alves, D. C. B.; Fujita, T.; Chen, M.; Asefa, T.; Shenoy, V. B.; Eda, G.; Chhowalla, M. Enhanced Catalytic Activity in Strained Chemically Exfoliated WS_2 Nanosheets for Hydrogen Evolution. *Nat. Mater.* **2013**, *12*, 850.
(46) Choi, Y.; Cho, J.; Lunsford, A. M.; Al-hashimi, M.; Fang, L.; Banerjee, S. Mapping the Electrocatalytic Activity of MoS_2 across Its

https://dx.doi.org/10.1021/acs.inorgchem.0c01648
Inorg. Chem. XXXX, XXX, XXX−XXX

Amorphous to Crystalline Transition. *J. Mater. Chem. A* **2017**, *5*, 5129−5141.
(47) Gao, M.; Xu, Y.; Jiang, J.; Yu, S. Nanostructured Metal Chalcogenides: Synthesis, Modification, and Applications in Energy Conversion and Storage Devices. *Chem. Soc. Rev.* **2013**, *42*, 2986−3017.
(48) Zeng, C.; Ramos-ruiz, A.; Field, J.; Sierra-alvarez, R. Cadmium Telluride (CdTe) and Cadmium Selenide (CdSe) Leaching Behavior and Surface Chemistry in Response to pH and O_2. *J. Environ. Manage.* **2015**, *154*, 78−85.
(49) Bhat, K. S.; Barshilia, H. C.; Nagaraja, H. S. Porous Nickel Telluride Nanostructures as Bifunctional Electrocatalyst towards Hydrogen and Oxygen Evolution Reaction. *Int. J. Hydrogen Energy* **2017**, *42*, 24645−24655.
(50) Wang, K.; Ye, Z.; Liu, C.; Zhou, C.; Shi, Z.; Xia, H.; Liu, G.; Qiao, G. Morphology-Controllable Synthesis of Cobalt Telluride Branched Nanostructures on Carbon Fiber Paper as Electrocatalysts for Hydrogen Evolution Reaction. *ACS Appl. Mater. Interfaces* **2016**, *8*, 2910−2916.
(51) Lu, T. H.; Chen, C. J.; Basu, M.; Ma, C. G.; Liu, R. S. $CoTe_2$ Nanostructure: An Efficient and Robust Catalyst for Hydrogen Evolution. *Chem. Commun.* **2015**, *51*, 17012−17015.
(52) Lu, C.; Wang, J.; Czioska, S.; Dong, H.; Chen, Z. Hierarchically Structured Cu-Based Electrocatalysts With Nanowires Array for Water Splitting. *J. Phys. Chem. C* **2017**, *121*, 25875−25881.
(53) Gillet, S.; Aguedo, M.; Petitjean, L.; Morais, A. R. C.; Da Costa Lopes, A. M.; Lukasik, R. M.; Anastas, P. T. Lignin Transformations for High Value Applications : Towards Targeted Modifications Using Green Chemistry. *Green Chem.* **2017**, *19*, 4200−4233.
(54) Sun, Z.; Fridrich, B.; de Santi, A.; Elangovan, S.; Barta, K. Bright Side of Lignin Depolymerization : Toward New Platform Chemicals. *Chem. Rev.* **2018**, *118*, 614−678.
(55) Wang, D.; Wang, P.; Wang, S.; Chen, Y.; Zhang, H.; Lai, A. Direct Electrochemical Oxidation of Alcohols with Hydrogen Evolution in Continuous-Flow Reactor. *Nat. Commun.* **2019**, *10*, 2796.
(56) Jiang, C.; Wang, H.; Wang, Y.; Ji, H. All Solid-State Z - Scheme $CeO_2/ZnIn_2S_4$ Hybrid for the Photocatalytic Selective Oxidation of Aromatic Alcohols Coupled with Hydrogen Evolution. *Appl. Catal., B* **2020**, *277*, 119235.
(57) Zhang, F.; Li, J.; Wang, H.; Li, Y.; Liu, Y.; Qian, Q.; Jin, X.; Wang, X.; Zhang, J.; Zhang, G. Realizing Synergistic effect of Electronic Modulation and Nanostructure Engineering over Graphitic Carbon Nitride for Highly efficient Visible-Light H_2 Production Coupled with Benzyl Alcohol Oxidation. *Appl. Catal., B* **2020**, *269*, 118772.
(58) Ko, M.; Pham, L. T. M.; Sa, Y. J.; Woo, J.; Nguyen, T. V. T.; Kim, J. H.; Oh, D.; Sharma, P.; Ryu, J.; Shin, T. J.; Joo, S. H.; Kim, Y. H.; Jang, J.-W. Unassisted Solar Lignin Valorisation Using a Compartmented Photo-Electro-Biochemical Cell. *Nat. Commun.* **2019**, *10*, 1−10.
(59) Anantharaj, S.; Ede, S. R.; Karthick, K.; Sam Sankar, S.; Sangeetha, K.; Karthik, P. E.; Kundu, S. Precision and Correctness in the Evaluation of Electrocatalytic Water Splitting: Revisiting Activity Parameters with a Critical Assessment. *Energy Environ. Sci.* **2018**, *11* (4), 744−771.
(60) Gorlin, Y.; Jaramillo, T. F. A Bifunctional Nonprecious Metal Catalyst for Oxygen Reduction and Water Oxidation. *J. Am. Chem. Soc.* **2010**, *132*, 13612−13614.
(61) Sridhar, K.; Chattopadhyay, K. Synthesis by Mechanical Alloying and Thermoelectric Properties of Cu_2Te. *J. Alloys Compd.* **1998**, *264*, 293−298.
(62) Han, C.; Li, Z.; Li, W.-j.; Chou, S.-l.; Dou, S.-x. Controlled Synthesis of Copper Telluride Nanostructures for Long-Cycling Anodes in Lithium Ion Batteries. *J. Mater. Chem. A* **2014**, *2*, 11683−116690.
(63) Li, W.; Zamani, R.; Gil, P. R.; Pelaz, B.; Ibanez, M.; Cadavid, D.; Shavel, A.; Alvarez-puebla, R. A.; Parak, W. J.; Arbiol, J.; Cabot, A. CuTe Nanocrystals: Shape and Size Control, Plasmonic Properties, and Use as SERS Probes and Photothermal Agents. *J. Am. Chem. Soc.* **2013**, *135*, 7098−7101.
(64) Pope, C. G. X-Ray Diffraction and the Bragg Equation. *J. Chem. Educ.* **1997**, *74*, 129−131.
(65) Joo, J. B.; Zhang, Q.; Dahl, M.; Lee, I.; Goebl, J.; Zaera, F.; Yin, Y. Control of the Nanoscale Crystallinity in Mesoporous TiO2 Shells for Enhanced Photocatalytic Activity. *Energy Environ. Sci.* **2012**, *5*, 6321−6327.
(66) Mondal, P.; Sinha, A.; Salam, N.; Roy, A. S.; Jana, N. R.; Islam, S. M. Enhanced Catalytic Performance by Copper Nanoparticle−Graphene Based Composite. *RSC Adv.* **2013**, *3*, 5615−5623.
(67) Gao, D.; Zhang, J.; Zhu, J.; Qi, J.; Zhang, Z.; Sui, W.; Shi, H.; Xue, D. Vacancy-Mediated Magnetism in Pure Copper Oxide Nanoparticles. *Nanoscale Res. Lett.* **2010**, *5*, 769−772.
(68) Xiao, Q.; Zhang, Y.; Guo, X.; Jing, L.; Yang, Z.; Xue, Y.; Yan, Y.-M.; Sun, K. A high-performance electrocatalyst for oxygen evolution reactions based on electrochemical post-treatment of ultrathin carbon layer coated cobalt nanoparticles. *Chem. Commun.* **2014**, *50*, 13019−13022.

https://dx.doi.org/10.1021/acs.inorgchem.0c01648
Inorg. Chem. XXXX, XXX, XXX−XXX